

Simplified stress analysis of multilayered adhesively bonded structures

Kübra Sekmen, Eric Paroissien, Frederic Lachaud

▶ **To cite this version:**

Kübra Sekmen, Eric Paroissien, Frederic Lachaud. Simplified stress analysis of multilayered adhesively bonded structures. International Journal of Adhesion and Adhesives, 2020, 97, pp.0. 10.1016/j.ijadhadh.2019.102497 . hal-02467848

HAL Id: hal-02467848
https://hal.science/hal-02467848

Submitted on 5 Feb 2020

HAL is a multi-disciplinary open access archive for the deposit and dissemination of scientific research documents, whether they are published or not. The documents may come from teaching and research institutions in France or abroad, or from public or private research centers.

L'archive ouverte pluridisciplinaire **HAL**, est destinée au dépôt et à la diffusion de documents scientifiques de niveau recherche, publiés ou non, émanant des établissements d'enseignement et de recherche français ou étrangers, des laboratoires publics ou privés.



Open Archive Toulouse Archive Ouverte (OATAO)

OATAO is an open access repository that collects the work of some Toulouse researchers and makes it freely available over the web where possible.

This is an author's version published in: https://oatao.univ-toulouse.fr/25080

Official URL: https://doi.org/10.1016/j.ijadhadh.2019.102497

To cite this version :

Sekmen, Kübra and Paroissien, Eric and Lachaud, Frédéric Simplified stress analysis of multilayered adhesively bonded structures. (In Press: 2020) International Journal of Adhesion and Adhesives, 97. ISSN 0143-7496

Any correspondence concerning this service should be sent to the repository administrator: tech-oatao@listes-diff.inp-toulouse.fr

Simplified stress analysis of multilayered adhesively bonded structures

Kubra Sekmen, Eric Paroissien *, Frédéric Lachaud

Institut Clément Ader (ICA), Université de Toulouse, ISAE-SUPAERO, INSA, IMT MINES ALBI, UTIII, CNRS, 3 Rue Caroline Aigle, 31400, Toulouse, France

Keywords:
Multilayered bonded joint
Semi-analytical resolution
Macro-element
Finite element stress analysis
Stress analysis
Stress distribution
Linear material adhesive

A B S T R A C T

Bolting technologies have been commonly used to assemble structural members in order to carry loads. However, the main drawback of these joints is the local reduction of the strength-to-stress ratio. Compared to the bolted joints, adhesive bonding technology allows for the increase of static and fatigue strength while reducing the weight. The Finite Element (FE) method is able to address the stress analysis of bonded joints. Nevertheless, analyses based on FE models are computationally expensive. Therefore, it is profitable to develop new simplified approaches enabling extensive parametric studies. A semi-analytical technique was developed to model the joints based on the formulation of 4-node special elements, termed macro-elements, which is able to simulate an entire bonded overlap at low computational costs. In this paper, a multilayered bonded-bars and a multilayered bonded-beams macro-elements are derived from bonded-bar and bonded-beam macro-elements. 1D-bar and 1D-beam simplified stress analyses of such multilayered joints are presented in order to predict the adhesive stress distributions along the overlap. For validation purpose, the results obtained by the simplified 1D-bar and 1D-beam model are compared with the results predicted by 1D-FE models. Good agreements are shown. Finally, the parametric studies are performed in order to understand the mechanical behavior of multilayered adhesively bonded structures. This presented simplified stress analysis can be used to deduce the sizing guidelines as a consequence of these parametric studies.

1. Introduction

In recent years, there has been an increasing interest in the adhesively bonded technology for the design of lightweight structures. Compared to the conventional methods such as riveting or bolting, bonding offers better mechanical properties in terms of stiffness, static strength and fatigue strength when joining without damaging dissimilar materials such as metals and composites [1–4]. The Finite Element (FE) method is able to address the stress analysis of bonded joints. However, since analyses based on FE models are computationally expensive, it would be profitable to develop new simplified approaches enabling extensive parametric studies. Numerous studies have attempted to perform simplified stress analysis and provided accurate predictions [5–7]. In 1938, Volkersen published the first stress analysis including the deformation of the adherends by the development of a shear lag model [8]. In 1944, Goland and Reissner developed the analysis of Volkersen by the first closed-form solution of adhesive stress distributions along the overlap for simply supported balanced joint made of adherend undergoing cylindrically bending [9]. The sandwich-type analysis concept was then employed by other researchers in order to improve this initial model considering different local equilibriums, different constitutive behaviors and various geometries [10–18]. The second and third authors of the present paper and their co-workers have been working on the development of the macro-element (ME) technique for the simplified stress analysis of bonded, bolted and hybrid (bonded/bolted) joints [19–29]. The ME technique is a semi-analytical resolution method inspired by the FE method and is developed to solve the system of differential equations considering the restrictions such as dissimilar adherends, various boundary conditions, and nonlinear adhesive material properties. A ME is then an element which includes physical properties of both adhesive layers and adherends as illustrated in Fig. 1. A number of researchers investigated the mechanism of load transfer in multilayered structures by using shear-lag theory. Nairn and Mendels proposed an optimal shear-lag method for the stress problems of the 2D planar layered structures [30]. Jiang and Peters derived a shear-lag model for 3D multilayered structures whose properties vary along the cross-section through the extension of Nairn and Mendels' study such as smart structures with embedded sensors and actuators [31]. Viet et al. also provided a new analytical model to predict the interlaminar shear stress in adhesively bonded multilayered metal laminates for the purpose of modeling layers of piezoelectric materials

* Corresponding author.
E-mail address: eric.paroissien@isae-supaero.fr (E. Paroissien).

https://doi.org/10.1016/j.ijadhadh.2019.102497

Nomenclature and units

A	matrix of the system of 1st order ODE coefficients
A_i	extensional stiffness (N) of adherend i
B_i	extensional and bending coupling stiffness (N.mm) of adherend i
D_i	bending stiffness (N.mm^2) of adherend i
$E_{a,i}$	adhesive Young's modulus (MPa) of adhesive i
E_i	adherend Young's modulus (MPa) of adherend i
F_e	vector of nodal forces
G_i	adhesive shear modulus (MPa) of the adhesive i
K_e	elementary stiffness matrix of multilayered macro-element
L	length (mm) of bonded overlap
M_e	matrix of nodal displacements
M_i	bending moment (N.mm) in the adherend i around the z-direction
N_e	matrix of nodal forces
N_i	normal force (N) in the adherend i in the x-direction
P	element nodal displacement vector
S_i	adhesive peel stress (MPa) in the adhesive i in the y-direction
S_{max}	maximal adhesive peel stress (MPa)
T_i	adhesive shear stress (MPa) in the adhesive i in the x-direction
T_{max}	maximal adhesive shear stress (MPa)
U_e	vector of nodal displacements
V_i	shear force (N) in the adherend i in the y-direction
Z	vector of normal forces and displacements for semi-analytical resolution
b	width (mm) of the adherends
e_i	thickness (mm) of adherend i
f	magnitude of applied tensile force (N)
h_i	half thickness (mm) of adherend i
k_I	adhesive elastic stiffness (MPa/mm) in the peel
k_{II}	adhesive elastic stiffness (MPa/mm) in shear
k_u	spring element stiffness (N/mm) along the x-axis
k_v	spring element stiffness (N/mm) along the y-axis
n_{BE}	number of bar or beam elements
n_{ME}	number of macro-elements
t_i	thickness (mm) of the adhesive layer i
t_{iFE}	thickness (mm) of the adhesive layer used in the FE model
u_i	displacement (mm) of adherend $i$in the $x$direction
v_i	displacement (mm) of adherend $i$in the $y$direction
Δ_i	overlap length (mm) of a macro-element
θ_i	bending angle (rad) of the adherend $i$around the z-direction
φ_A	vector of normal forces and displacements at each extremity
φ_F	vector of normal forces each extremity
φ_U	vector of displacements at each extremity
$\nu_{a,i}$	Poisson's ratio of the adhesive layers
(x,y,z)	global reference system of axes
FE	Finite Element
ME	macro-element
ODE	ordinary differential equation

on the future energy harvesting application [32]. Recently, Pham et al. developed a FE formulation for the analysis of multilayered beams based on the principle of stationary complementary strain energy which differs from previous studies [33].

Literature reviews have indicated that plenty of models of the adhesively bonded joints have been developed to size simple configurations. Although the effectiveness of the adhesively bonded joint is widely known, the stress analysis and sizing methodologies of multilayered structures have not been extensively studied. Since studies on the stress analysis and sizing of the multilayered structures are rare to find in literature, the semi-analytical analysis in applying well-known schemes and parametric studies are performed in this work.

The objectives of the present paper are to perform the simplified stress analysis of the multilayered adhesively bonded joint under the static loading and to conduct parametric studies in order to understand their effects on the mechanical behavior of such joints. First of all, simplified stress analyses based on ME technique in 1D-bar and 1D-beam framework explained. The detailed mathematical description of semi-analytical resolution is provided. Then, 1D-FE models are presented and used to validate 1D-ME models through dedicated convergence studies. Finally, the parametric studies are performed in order to understand the mechanical behavior of such joints. The computations were performed thanks to house-made computer programs developed in MATLAB. Codes are provided as supplementary materials [34].

2. Description of simplified stress analyses of multilayered bonded joints

2.1. Overview of the macro-element technique and application

The simplified linear elastic method is originally developed for the hybrid (bolted/bonded) joints [21,22]. The ME technique is a mathematical procedure inspired by the FE method. When the ME technique takes the shape of solutions of the governing ordinary differential equations (ODEs) systems, it differs from the common FE method because of the fact that the interpolation functions are not assumed. This method allows for the resolution of the system of ODEs, which are derived from the constitutive equations of the adhesives and adherends and local equilibrium equations, under a less restricted application field of the simplifying hypotheses in terms of the geometry, material behavior, kinematics, boundary conditions and applied loads. A direct outcome is that only one ME is sufficient to mesh a complete bonded overlap. The main work is the formulation of the elementary stiffness matrix of the multilayered bonded elements. A multilayered bonded-bars and a multilayered bonded-beams MEs are derived based on the formulation of 4-nodes bonded-bar and bonded-beam elements. In this work, the formulation is based on the exponential matrix to solve the system of first order ODEs and then to derive the elementary stiffness matrix of these ODEs. As a result, in order to assess the adherend displacements, internal forces and adhesive stresses, an entire bonded overlap is meshed using dedicated MEs. According to FE rules, the global stiffness matrix of the complete structure is assembled from the elementary stiffness matrices of the macro-elements. Boundary conditions and prescribed loadings are applied through the Augmented Lagrangian Method [34]. Based on the minimization of the total potential energy, the linear system is solved in order to compute the

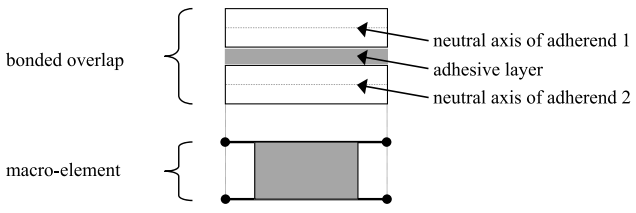


Fig. 1. Equivalent modeling of a bonded overlap by a macro-element.

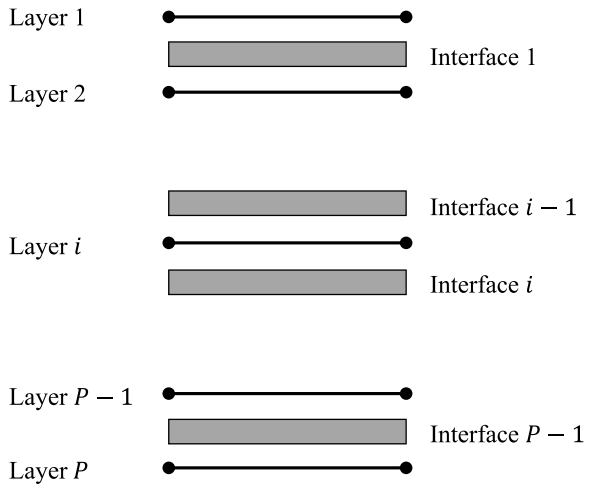


Fig. 2. Representation of the nomenclature for the ME of multilayered joint.

displacements and forces in the adherends as well as the adhesive shear and peel stresses. Finally, different mechanical loading could be easily taken into account.

2.2. D-bar and 1D-beam element model

2.2.1. Bonded-bars element: 1D-bar kinematics

The following hypotheses were taken (i) the adherends are linear elastic materials simulated as 1D-bars, (ii) the adhesive layer is simulated by an infinite number of linear elastic shear springs linking the adherends (iii) the thickness of the adhesive layer is constant along the overlap, and (iv) the adhesive stresses are constant through the thickness [8]. As a consequence of the simplified hypotheses, the following arguments are taken into consideration (i) only normal forces and only longitudinal displacements are considered in the adherend, (ii) the adhesive normal stress cannot be represented because any normal force is not applied to the adhesive layer, and (iii) it is assumed that all the adhesive stress components disappear except the in-plane shear. The ME is formed of a total of Padherends which are linked by $P-1$interfaces representing adhesive layers. The nomenclature of ME for a multilayered adhesively bonded joint is described as shown in Fig. 2. The nodes of the ME are located on the neutral axis of each layer. Each layer has 2 nodes which are located on the starting and end of the layers. Thus, a ME including Players has $2P$nodes in total. Within the scope of 1D-bar kinematics, there is 1° of freedom which is longitudinal displacement. The total number of degrees of freedom is computed by multiplying a total of nodes with a degree of freedom per nodes. As a result, 1 ME of Players includes a total of $2P$degrees of freedom. In this model, nodes at the interfaces are not modeled. The modeling of each layer as a bar allows for the computation of the longitudinal displacements, normal forces, normal stresses, and strains.

The local equilibrium of the adherends belongs to the Volkersen type. Based on the free body diagram of infinitesimal pieces included between $x$and $x+dx$of Padherends in the overlap region as presented in Fig. 3, one equation is obtained for each layer. As a result, a total of Pequations are obtained for Players.

The local equilibrium equations are given for 1^{st}, $i^{th}(2\leq i\leq P-1)$ and P^{th}adherend:

$$\begin{cases} \dfrac{dN_1}{dx}+T_1 b=0 \\ \dfrac{dN_i}{dx}-(T_{i-1}-T_i)b=0 \\ \dfrac{dN_P}{dx}-T_{P-1}b=0 \end{cases} \tag{1}$$

where $N_i$is the normal force in the adherend i, $b$the width of the adherends and $T_i$the adhesive shear stress.

One constitutive equation for the adhesive shear stress describes each interface behavior. Then, a total of $P-1$equations are involved. For $1\leq i\leq P-1$, the linear elastic material behavior provides the constitutive equations of interfaces are below:

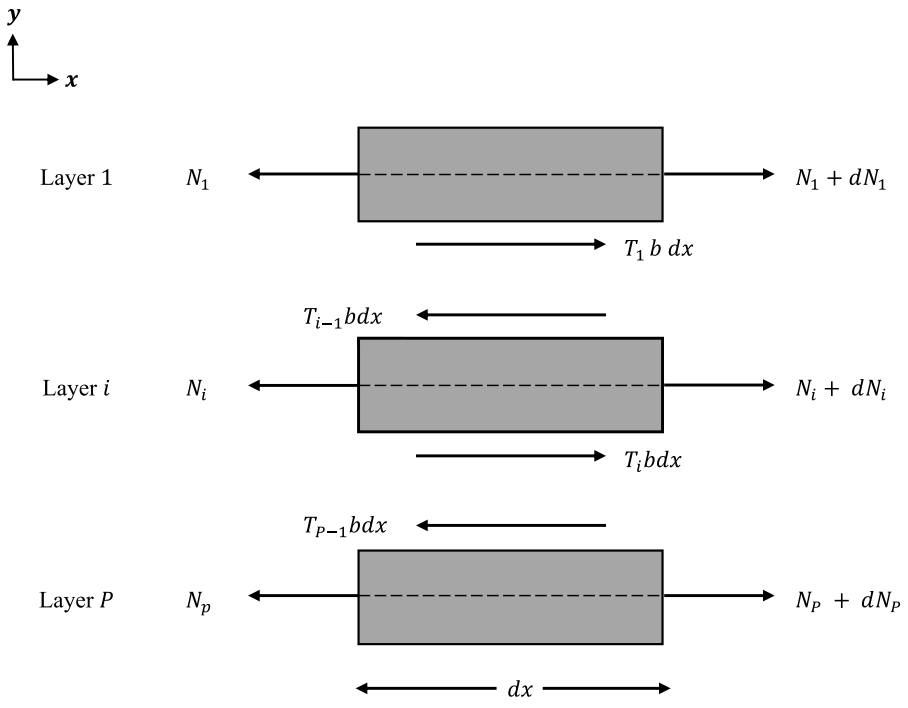


Fig. 3. Free body diagram of infinitesimal pieces included between $x$and $x+dx$of Padherends in the overlap region.

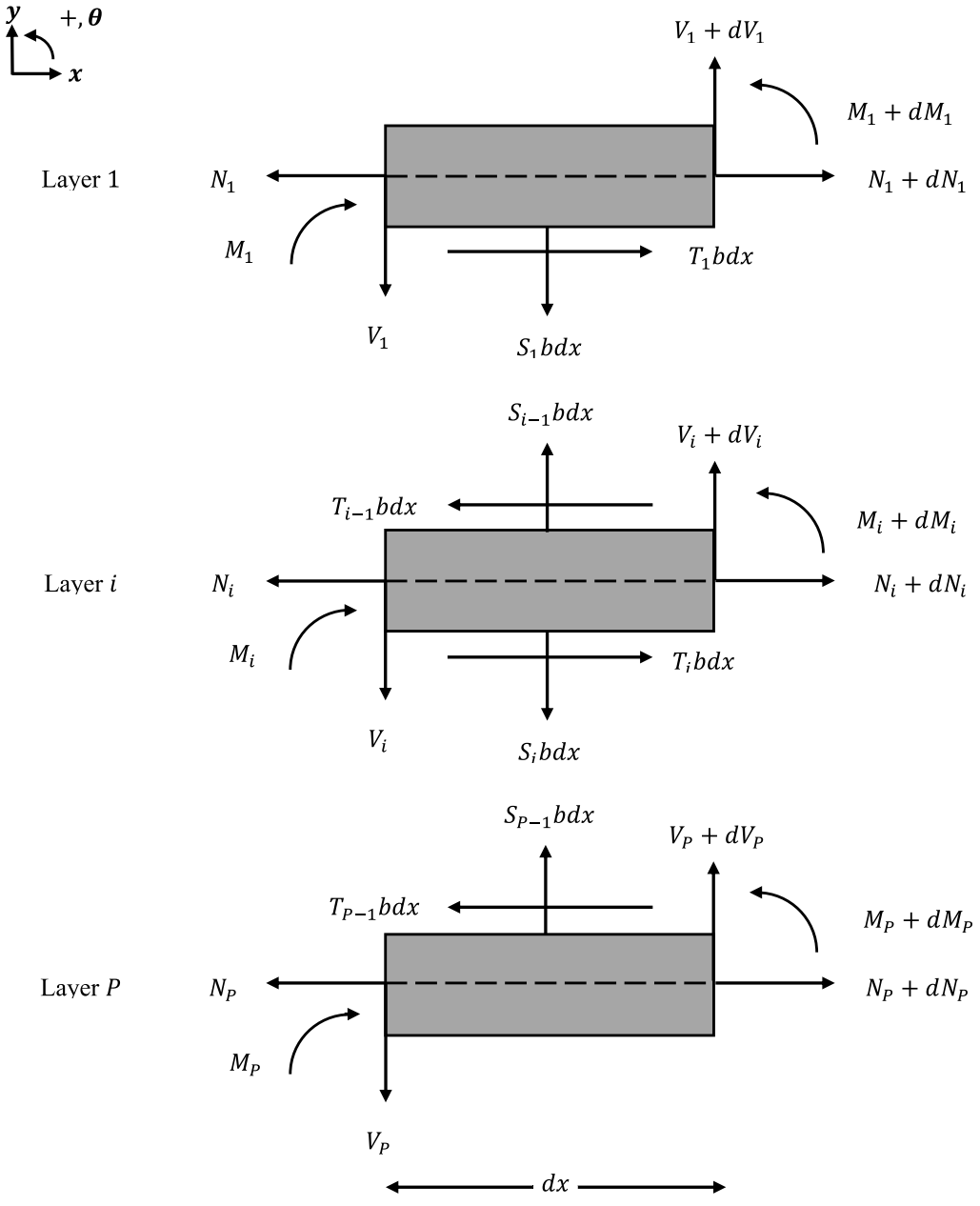


Fig. 4. Free body diagram of infinitesimal pieces included between *x*and $x + dx$of *P*adherends in the overlap region.

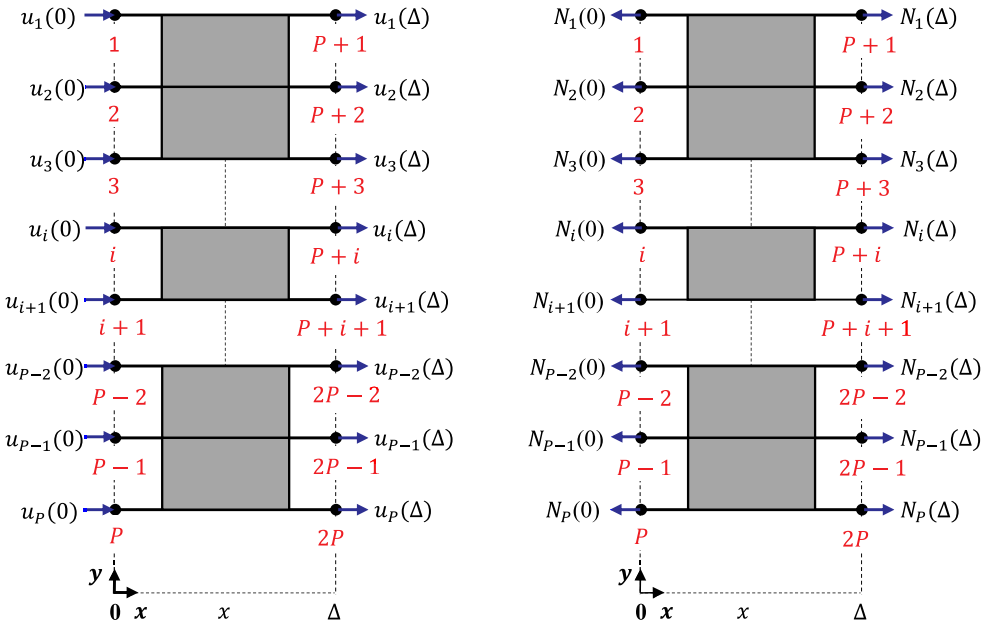


Fig. 5. Illustration of a multilayered bonded-bars element for nodes numbering, nodal displacements and nodal forces.

$$T_i = \frac{G_i(u_{i+1} - u_i)}{t_i} \tag{2}$$

where $t_i$is the thickness of adhesive layer i, $G_i$is the shear modulus of adhesive layer i, $u_i$is the normal displacement of points located at the abscissa $x$on the neutral line of adherend $i$before deformation.

The constitutive equations for the adherends ($1 \leq i \leq P$) are provided by:

$$N_i = E_i b e_i \frac{du_i}{dx} \quad \Rightarrow \quad \frac{du_i}{dx} = \frac{1}{E_i b e_i} N_i \tag{3}$$

where $E_i$is Young's modulus of the adherend $i$and $e_i$the thickness of the adherend i.

The ODEs are organized in order to get the expression for displacements and then for internal forces by the resolution. Substituting Eq. (2) into Eq. (1), the following local equilibrium equations are obtained:

$$\begin{cases} \dfrac{dN_1}{dx} = b\dfrac{G_1}{t_1}u_1 - b\dfrac{G_1}{t_1}u_2 \\ \dfrac{dN_i}{dx} = -b\dfrac{G_{i-1}}{t_{i-1}}u_{i-1} + b\left(\dfrac{G_{i-1}}{t_{i-1}} + \dfrac{G_i}{t_i}\right)u_i - b\dfrac{G_i}{t_i}u_{i+1} \\ \dfrac{dN_P}{dx} = -b\dfrac{G_{P-1}}{t_{P-1}}u_{P-1} + b\dfrac{G_{P-1}}{t_{P-1}}u_P \end{cases} \tag{4}$$

2.2.2. *Bonded-beams element: 1D-beam kinematics*

The set of simplifying hypotheses are: (i) the adherends are simulated by linear elastic 1D Euler-Bernoulli laminated beams, (ii) the adhesive layer is simulated by an infinite number of elastic shear and transverse springs linking the adherends, (iii) the thickness of the adhesive layer is constant along the overlap, and (iv) the adhesive stresses are constant through the thickness [9]. As a consequence of the simplified hypothesis, the following arguments are taken into consideration (i) normal forces, shear forces and bending moments are considered in the adherends, (ii) longitudinal displacements, deflections and bending angles are considered in the adherends, (iii) adhesive shear and peel stresses are represented in the adherends, and (iv) the adhesive longitudinal stresses are neglected. Similar to 1D-bar model, the ME is formed by Padherends and $P-1$interfaces. The nomenclature of ME for a multilayered adhesively bonded joint is presented as given in Fig. 2. Within the scope of 1D-beam kinematics, there are 3° of freedom which are axial displacement, vertical displacement, and rotation. The total number of degrees of freedom is computed by multiplying a total of nodes with a degree of freedom per nodes. As a result, one ME of Players includes a total of $6P$degrees of freedom. Similar to 1D-bar model, nodes at the interfaces are not modeled in 1D-beam model. The local equilibrium of the adherends belongs to Goland and Reissner type. Based on the free body diagram of infinitesimal pieces included between $x$and $x+dx$of Padherends in the overlap region as shown in Fig. 4, three equations are obtained for each layer. As a result, a total of $3P$equations are obtained for Players. The half thickness of the adherend $i$are termed h_i:

$$h_i = \frac{e_i}{2}, \quad i = 1, \ldots, P \tag{5}$$

The local equilibrium equations are given for 1st, $i^{th}(2 \leq i \leq P-1)$ and P^{th}adherend:

$$\begin{cases} \dfrac{dN_1}{dx} + T_1 b = 0 \\ \dfrac{dV_1}{dx} - S_1 b = 0 \\ \dfrac{dM_1}{dx} + V_1 + T_1 b h_1 = 0 \\ \dfrac{dN_i}{dx} - (T_{i-1} - T_i)b = 0 \\ \dfrac{dV_i}{dx} + (S_{i-1} - S_i)b = 0 \\ \dfrac{dM_i}{dx} + V_i + (T_{i-1} + T_i)b h_i = 0 \\ \dfrac{dN_P}{dx} - T_{P-1} b = 0 \\ \dfrac{dV_P}{dx} + S_{P-1} b = 0 \\ \dfrac{dM_P}{dx} + V_P + T_{P-1} b h_P = 0 \end{cases} \tag{6}$$

where $N_i$is the normal force in the adherend i, $V_i$the shear force in the adherend i, $M_i$bending moment in the adherend i, $b$the width of the adherend, $T_i$the adhesive shear stress in the adhesive $i$and $S_i$the adhesive peel stress in the adhesive i.

Two constitutive equations regarding the adhesive stresses describe

each interface behavior. Then, a total of $2(P-1)$equations are involved. For $1 \leq i \leq P-1$, the linear elastic material behavior provides the constitutive equation of interfaces as functions of adherends displacements are below:

$$\begin{cases} S_i = k_{I,i}(w_i - w_{i+1}) \\ T_i = k_{II,i}(u_{i+1} - u_i - h_{i+1}\theta_{i+1} - h_i\theta_i) \end{cases} \tag{7}$$

where $k_{I,i} = \frac{E_{a,i}}{t_i}$is adhesive elastic stiffness in the peel, $k_{II,i} = \frac{G_i}{t_i}$adhesive elastic stiffness in the shear, $t_i$the thickness of the adhesive i, $E_{a,i}$the elastic modulus of the adhesive i, $G_i$the shear modulus of the adhesive i, $u_i$the axial displacement of the adherend i, $w_i$the deflection of the adherend $i$and $\theta_i$the bending angle of the adherend i.

The constitutive equations for the adherends $(1 \leq i \leq P)$are provided by:

$$\begin{cases} N_i = A_i\dfrac{du_i}{dx} - B_i\dfrac{d\theta_i}{dx} \Rightarrow \dfrac{du_i}{dx} = \dfrac{D_i}{\Omega_i}N_i + \dfrac{B_i}{\Omega_i}M_i \\ M_i = -B_i\dfrac{du_i}{dx} + D_i\dfrac{d\theta_i}{dx} \Rightarrow \dfrac{d\theta_i}{dx} = \dfrac{B_i}{\Omega_i}N_i + \dfrac{A_i}{\Omega_i}M_i \\ \theta_i = \dfrac{dw_i}{dx} \end{cases} \tag{8}$$

where $A_i$is the extensional stiffness of the adherend i, $D_i$the bending stiffness of the adherend i, $B_i$the extensional and bending coupling stiffness of the adherend $i$and $\Omega_i = A_iD_i - B_iB_i$is different from zero for $i = 1,\ldots,P$.

Substituting Eq. (7) into Eq. (6), the following local equilibrium equations are obtained:

$$\begin{cases} \dfrac{dN_1}{dx} = -bk_{II,1}(u_2 - u_1 - h_2\theta_2 - h_1\theta_1) \\ \dfrac{dV_1}{dx} = bk_{I,1}(w_1 - w_2) \\ \dfrac{dM_1}{dx} = -V_1 - bh_1k_{II,1}(u_2 - u_1 - h_2\theta_2 - h_1\theta_1) \\ \dfrac{dN_i}{dx} = bk_{II,i-1}(u_i - u_{i-1} - h_i\theta_i - h_{i-1}\theta_{i-1}) - bk_{II,i}(u_{i+1} - u_i - h_{i+1}\theta_{i+1} - h_i\theta_i) \\ \dfrac{dV_i}{dx} = -bk_{I,i-1}(w_{i-1} - w_i) + bk_{I,i}(w_i - w_{i+1}) \\ \dfrac{dM_i}{dx} = -V_i - bh_ik_{II,i-1}(u_i - u_{i-1} - h_i\theta_i - h_{i-1}\theta_{i-1}) - bh_ik_{II,i}(u_{i+1} - u_i - h_{i+1}\theta_{i+1} - h_i\theta_i) \\ \dfrac{dN_P}{dx} = bk_{II,P-1}(u_P - u_{P-1} - h_P\theta_P - h_{P-1}\theta_{P-1}) \\ \dfrac{dV_P}{dx} = -bk_{I,P-1}(w_{P-1} - w_P) \\ \dfrac{dM_P}{dx} = -V_P - bh_Pk_{II,P-1}(u_P - u_{P-1} - h_P\theta_P - h_{P-1}\theta_{P-1}) \end{cases} \tag{9}$$

2.3. Semi-analytical resolution

The formulation of elementary stiffness matrices of the multilayered bonded-bars element and the multilayered bonded-beams element is derived from the linear relationship between the vector of nodal forces $F_e$and the vector of the nodal displacements U_e. The elementary stiffness matrices for multilayered bonded-bars element and multilayered bonded-beams element $K_e$are provided in Eqs. (10) and (11), respectively.

$$\begin{pmatrix} -N_1(0) \\ -N_i(0) \\ -N_p(0) \\ N_1(\Delta) \\ N_i(\Delta) \\ N_P(\Delta) \end{pmatrix} = K_e \begin{pmatrix} u_1(0) \\ u_i(0) \\ u_p(0) \\ u_1(\Delta) \\ u_i(\Delta) \\ u_P(\Delta) \end{pmatrix} \Leftrightarrow F_e = K_eU_e \tag{10}$$

where $\Delta$is the length of the ME.

In the case of 1D-bar and 1D-beam kinematics, the semi-analytical resolution is carried out using the ME technique in order to determine the elementary stiffness matrices.

2.4. Multilayered bonded-bars element

The system of first order ODEs, which are derived from Eqs. (3) and (4) can be written under a matrix shape such as:

$$\left\{\frac{dZ}{dx}\right\} = [A]\{Z\} \tag{12}$$

where $Z = (N_1 \ldots N_i \ldots N_P \;\; u_1 \ldots u_i \ldots u_P)^T$.

The solution of the system is under the shape of the exponential of the matrix as shown in Eq. (13).

$$Z = expm(Ax).Z_0 \tag{13}$$

where $\{Z_0\}$is the vector constant.

The ME of the multilayered bonded-bars is modeled as illustrated in Fig. 5. From the first layer to the last layer P, all layers are assembled one under the other. Node numbering is provided as layer by layer in order to obtain one multilayered ME. The numbering of degrees of freedom of the ME is started with the first node of each layer, and it is done from the top layer to the bottom layer. Then, after reaching the first node of the last layer, numbering proceeds from the second nodes of the first layer to the last layer. One multilayered bonded-bars element has a total of $2P$nodes, $2Px1$degrees of freedom, $P-1$adhesive layers, and Padherends.

The elementary stiffness matrix of a multilayered bonded-bars element has to be determined. The implementation of the elementary stiffness matrix is carried out by MATLAB software. The MATLAB provides the possibility to compute the exponential of a matrix by means of the function “expm”. The following steps have been used to obtain the

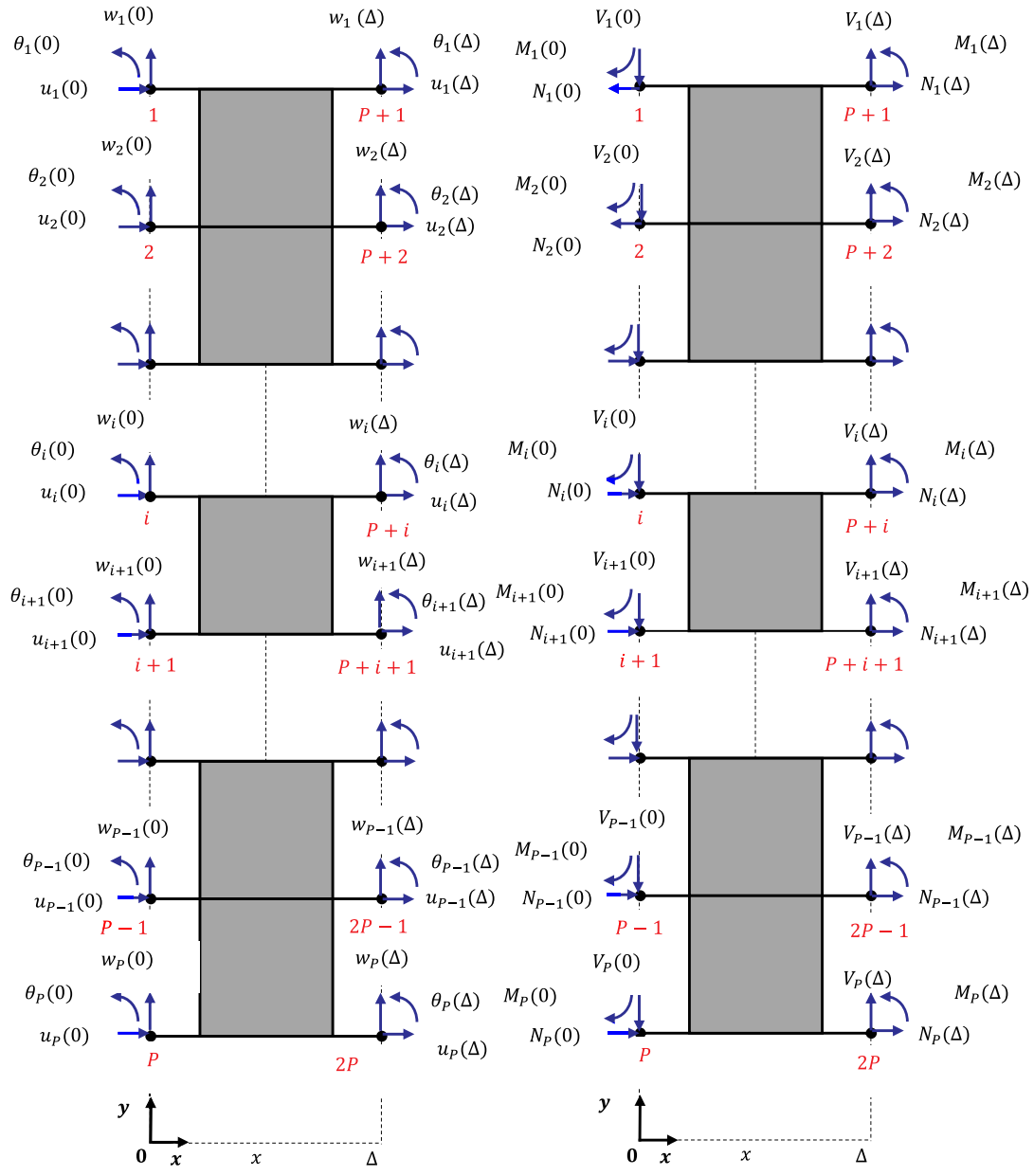


Fig. 6. Illustration of a multilayered bonded-beams element for nodes numbering, nodal displacements and nodal forces.

multilayered bonded bar element stiffness matrix. Firstly, the boundary conditions at both extremities of the ME in $x = 0$and $x = \Delta$lead to the expressions of fundamental $6P\ x\ 6P$matrices.

$$\varphi_A(x=0) = EXPm(Ax0)_{6PX6P} \tag{14}$$

$$\varphi_A(x=\Delta) = EXPm(Ax\Delta)_{6Px6P} \tag{15}$$

Each line of these matrices indicates each line of the vector $(N\ u)^T$which is computed at each extremity in $x = 0$and $x = \Delta$Secondly, $3P\ x\ 6P$matrices referring to displacements Uonly and forces Fonly at each extremity are computed.

$$\varphi_U(0,\Delta) = \begin{bmatrix} EXPm(Ax0)_{i=4P:6P,j=1:6P} \\ EXPm(Ax\Delta)_{i=4P:6P,j=1:6P} \end{bmatrix}_{(u_1(0)\ldots\ u_i(0)\ldots\ u_P(0)\ u_1(\Delta)\ldots\ u_i(\Delta)\ldots\ u_P(\Delta))^T} \tag{16}$$

$$\varphi_F(0,\Delta) = \begin{bmatrix} EXPm(Ax0)_{i=1P:3P,j=1:6P} \\ EXPm(Ax\Delta)_{i=1P:3P,j=1:6P} \end{bmatrix}_{(N_1(0)\ldots\ N_i(0)\ldots\ N_P(0)\ N_1(\Delta)\ldots\ N_i(\Delta)\ldots\ N_P(\Delta))^T} \tag{17}$$

Thirdly, $6P\ x\ 6P$matrix $M_e$of nodal displacements is reordered in the base

$$(u_1(0)\ u_1(\Delta)\ \ldots u_i(0)\ u_i(\Delta)\ \ldots u_P(0)\ u_P(\Delta))^T$$

instead of $(u_1(0)\ldots\ u_i(0)\ldots\ u_P(0)\ u_1(\Delta)\ldots\ u_i(\Delta)\ldots\ u_P(\Delta))^T$.

$$M_e = \begin{bmatrix} EXPm(Ax0)_{i=4P:6P,j=1:6P} \\ EXPm(Ax\Delta)_{i=4P:6P,j=1:6P} \end{bmatrix}_{(u_1(0)\ u_1(\Delta)\ \ldots u_i(0)\ u_i(\Delta)\ \ldots u_P(0)\ u_P(\Delta))^T} \tag{18}$$

$6P\ x\ 6P$matrix $N_e$of nodal forces is also reordered in the base

$$(-N_1(0)\ N_1(\Delta)\ \ldots -N_i(0)\ N_i(\Delta)\ \ldots -N_P(0)\ N_P(\Delta))^T$$

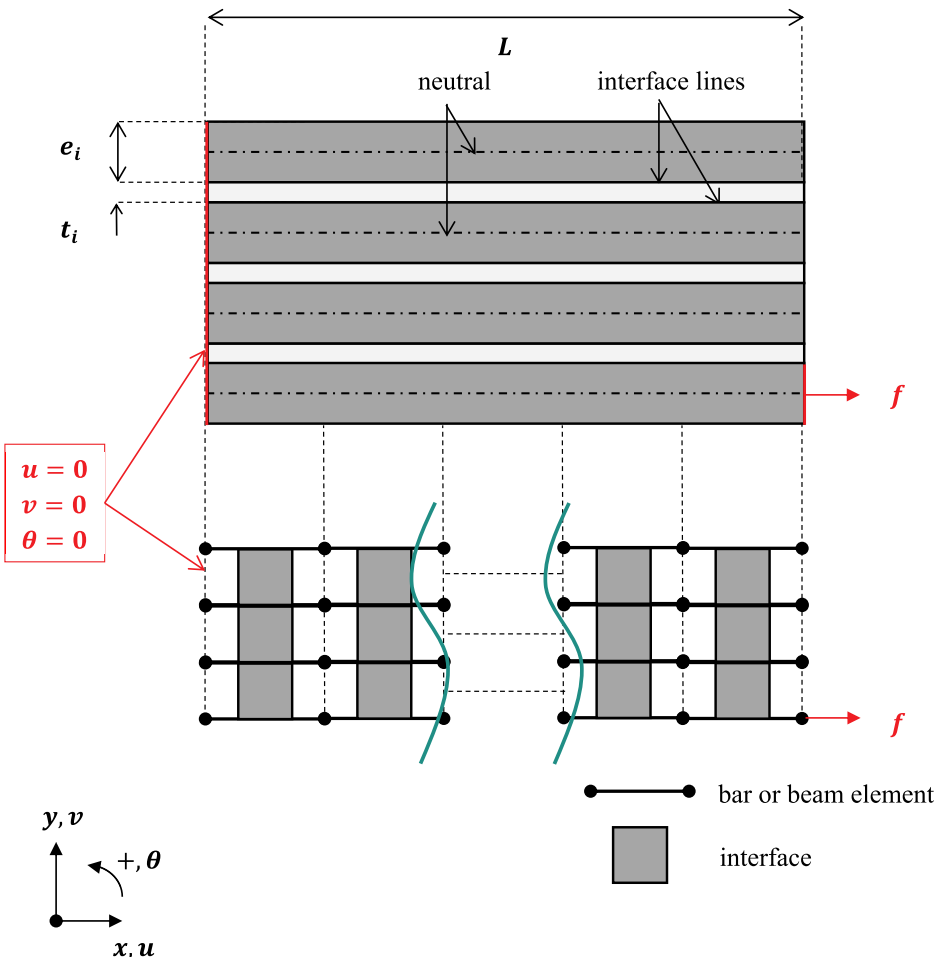


Fig. 7. Multilayered bonded joint for $P = 4$with principle scheme of the ME.

Table 1
Geometrical parameters of joint configuration.

Length of the overlap	L	30 mm
Width of the adherends	b	1 mm
Thickness of the adherends	e_i	2.5 mm
Thickness of the adhesives	t_i	0.11 mm

Table 2
Material parameters of the adherends and adhesives.

Young's modulus of adherends	E_i	70 GPa
Shear modulus of the adhesives	G_i	100 MPa
Poisson's ratio of the adhesives	$\nu_{a,i}$	0.3
Young's modulus of the adhesives	$E_{a,i}$	266 MPa

Table 3
Mechanical analysis parameters.

Applied force	f	100 N
Number of adherend layers	P	4

instead of $(N_1(0)\ldots N_i(0)\ldots N_P(0)\ N_1(\Delta)\ldots N_i(\Delta)\ldots N_P(\Delta))^T$.

$$N_e = \begin{bmatrix} EXPm(Ax0)_{i=4P:6P,j=1:6P} \\ EXPm(Ax\Delta)_{i=4P:6P,j=1:6P} \end{bmatrix}_{(-N_1(0)\ N_1(\Delta)\ \ldots -N_i(0)\ N_i(\Delta)\ \ldots -N_P(0)\ N_P(\Delta))^T} \tag{19}$$

Finally, the stiffness matrix is then computed by the following product of matrices.

$$[K_e] = [N_e][M_e]^{-1} \tag{20}$$

2.4.1. *Multilayered bonded-beams element*

Similar to the multilayered bonded-bars element, the system of first order ODEs, which are derived from Eqs. (8) and (9), can be written under a matrix shape in Eq. (12) where $Z = (N_1\ldots N_i\ldots N_P\ V_1\ldots V_i\ldots V_P\ u_1\ldots u_i\ldots u_P\ w_1\ldots w_i\ldots w_P\ \theta_1\ldots\theta_i\ldots\theta_P)^T$.

The solution of the system is under the shape of the exponential of the matrix as shown in Eq. (13). The ME of the multilayered bonded-beams is modeled as illustrated in Fig. 6. The elementary stiffness matrix of a multilayered bonded-beams element has to be determined. The following steps have been used to obtain the multilayered beam element stiffness matrix. First of all, the boundary conditions at both extremities of the ME in $x = 0$and $x = \Delta$lead to the expressions of fundamental $6P\ x\ 6P$matrices.

$$\varphi_A(x=0) = EXPm(Ax0)_{6PX6P} \tag{21}$$

$$\varphi_A(x=\Delta) = EXPm(Ax\Delta)_{6Px6P} \tag{22}$$

Each line of these matrices indicates each line of the vector $(N\ V\ M\ u\ w\ \theta)^T$which is computed at each extremity in $x = 0$and $x = \Delta$Then, $3P\ x\ 6P$matrices referring to displacements Uonly and forces Fonly at each extremity are computed.

$$\varphi_U(0,\Delta) = \begin{bmatrix} EXPm(Ax0)_{i=4P:6P,j=1:6P} \\ EXPm(Ax\Delta)_{i=4P:6P,j=1:6P} \end{bmatrix}_{(u_0\ w_0\ \theta_0\ u_\Delta\ w_\Delta\ \theta_\Delta)^T} \tag{23}$$

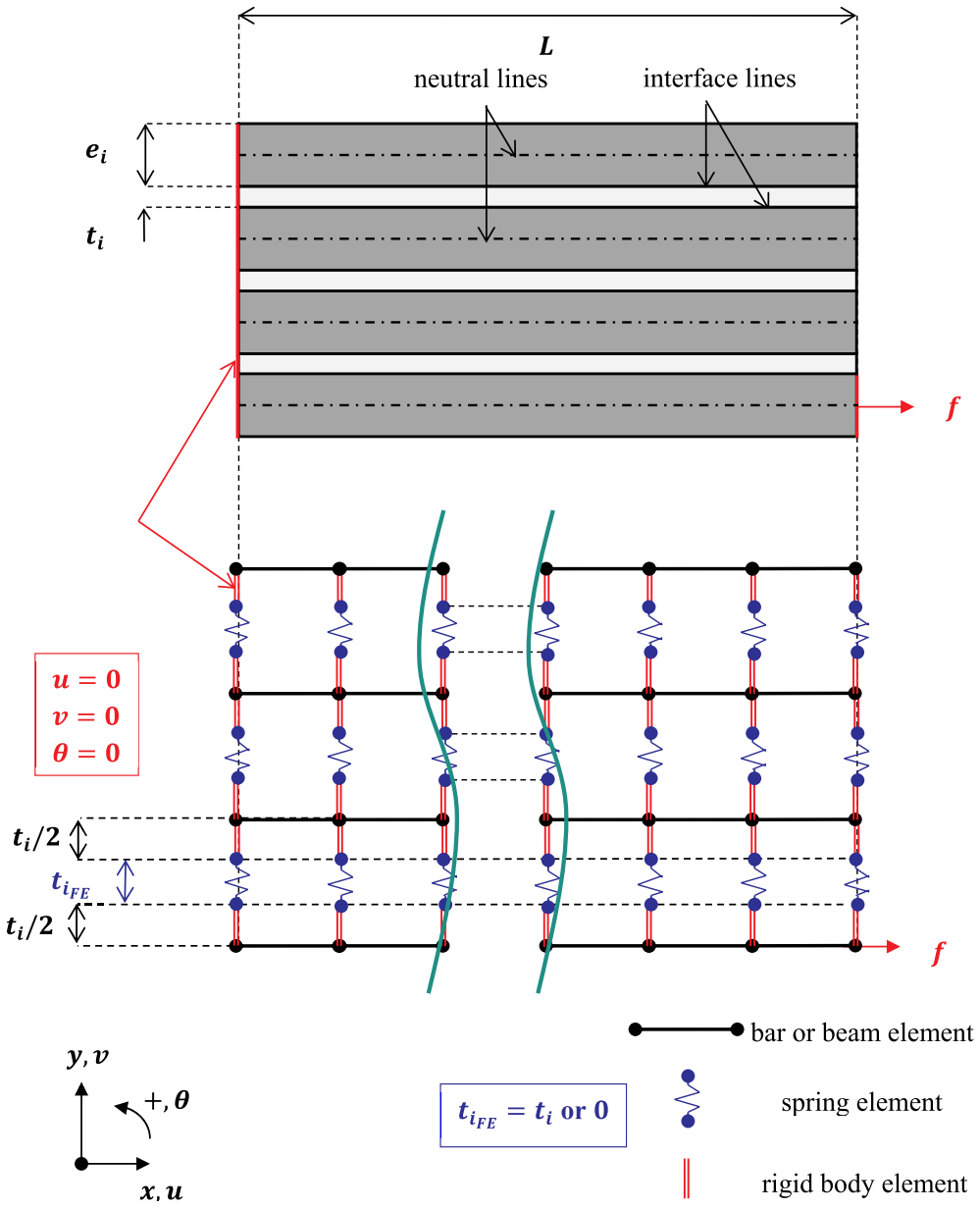


Fig. 8. Principle scheme for 1D-FE models.

$$\varphi_F(0,\Delta) = \begin{bmatrix} EXPm(Ax0)_{i=1P:3P,j=1:6P} \\ EXPm(Ax\Delta)_{i=1P:3P,j=1:6P} \end{bmatrix}_{(N_0\ V_0\ M_0\ N_\Delta\ V_\Delta\ M_\Delta)^T} \tag{24}$$

After that, $6P\,x\,6P$matrix $M_e$of nodal displacements is reordered in the base $(u_0\ u_\Delta\ w_0\ w_\Delta\ \theta_0\ \theta_\Delta)^T$instead of $(u_0\ w_0\ \theta_0\ u_\Delta\ w_\Delta\ \theta_\Delta)^T$.

$$M_e = \begin{bmatrix} EXPm(Ax0)_{i=4P:6P,j=1:6P} \\ EXPm(Ax\Delta)_{i=4P:6P,j=1:6P} \end{bmatrix}_{(u_0\ u_\Delta\ w_0\ w_\Delta\ \theta_0\ \theta_\Delta)^T} \tag{25}$$

$6P\,x\,6P$matrix $N_e$of nodal forces is also reordered in the base $(-N_0\ N_\Delta\ -V_0\ V_\Delta\ -M_0\ M_\Delta)^T$instead of $(N_0\ V_0\ M_0\ N_\Delta\ V_\Delta\ M_\Delta)^T$.

$$N_e = \begin{bmatrix} EXPm(Ax0)_{i=4P:6P,j=1:6P} \\ EXPm(Ax\Delta)_{i=4P:6P,j=1:6P} \end{bmatrix}_{(-N_0\ N_\Delta\ -V_0\ V_\Delta\ -M_0\ M_\Delta)^T} \tag{26}$$

Finally, the stiffness matrix is then computed by the following product of matrices.

$$[K_e] = [N_e][M_e]^{-1} \tag{27}$$

3. Validation

For validation purpose, the relevance of 1D-bar model is assessed in order to understand if the method is well-implemented. Then, the predictions obtained by the simplified 1D-bar and 1D-beam ME model are compared with the results predicted by 1D-FE models.

3.1. Nominal test case

In this paper, a clamped-free end multilayered joint subjected to in-plane tensile loading with a force f. This axial force is applied to the P^{th}layer at $x = L$where $L$is the length of the overlap. The bonded overlap is regularly meshed with $n_{ME}$of multilayered bonded-bars and multilayered bonded-beams elements. The number of adherends is chosen $P = 4$in order to perform the stress analysis as given in Fig. 7 with the ME scheme. The material, geometrical and mechanical analysis parameters are provided in Tables 1–3, respectively.

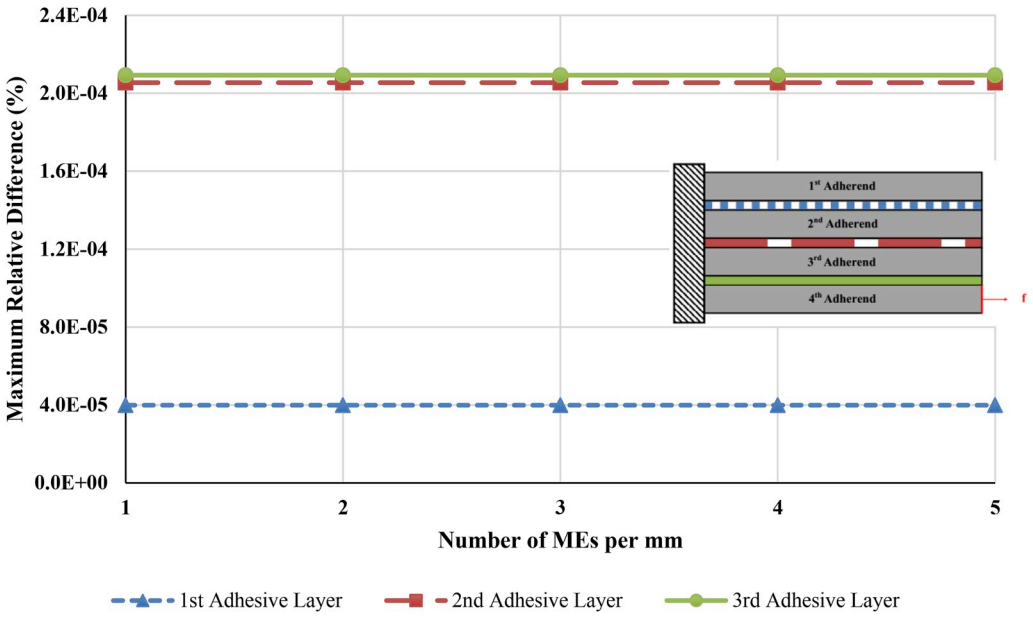


Fig. 9. Maximum relative difference between FE and ME adhesive peak shear stress predictions by 1D-bar model in terms of the number of MEs used per mm.

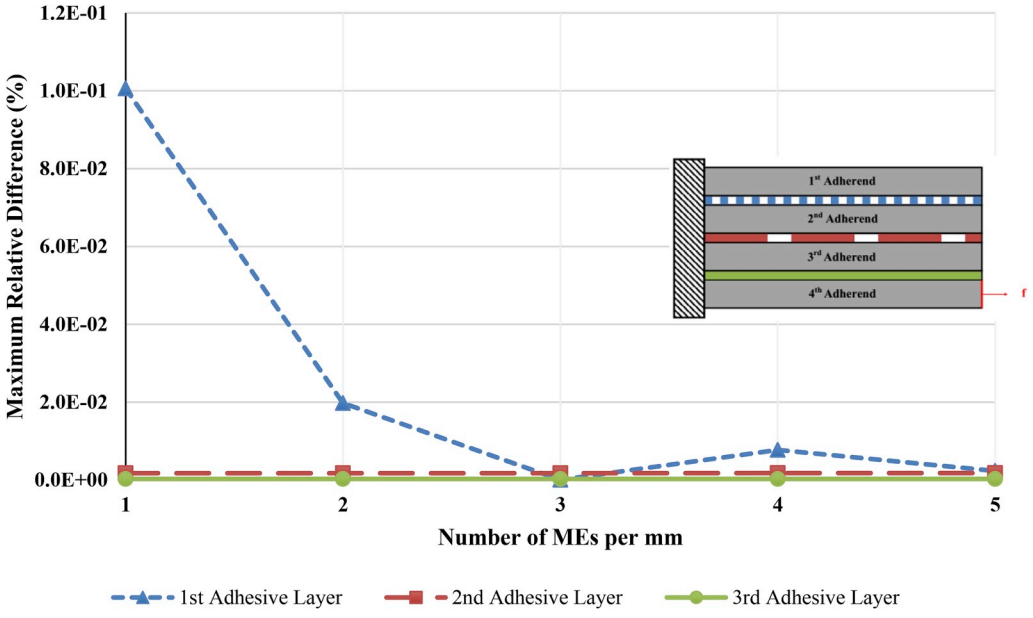


Fig. 10. Maximum relative difference between FE and ME adhesive peak shear stress predictions by 1D-beam model in terms of the number of MEs used per mm.

3.2. Description of the FE model

The FE models are designed considering the same hypotheses as ME models in order to justify the developed models [29]. This FE model is applied to a particular case in order to study the mechanical analysis of multilayered joints. 1D-FE models were developed by bar or beam elements for the adherends and spring element for the adhesive layers. The nodes associated with the bar and beam elements are located at the actual neutral line of the adherend. The nodes associated with the spring elements are located at the actual interfaces of the adherends. Rigid body elements are used in order to link the nodes of the neutral lines to the nodes of the adherend interface for each adherends along the overlaps. A scheme of the 1D-FE model is presented in Fig. 8 including prescribed displacements and loading. It is possible to consider the geometrical effect of the adhesive thickness by assigning $t_{iFE} = t_i$instead of $t_{iFE} = 0$. The bar and beam elements are based on third degree interpolating functions under the Euler-Bernoulli kinematics. The overlap length is regularly meshed by n_{BE}. The stiffnesses of springs $k_{u,i}$and $k_{v,i}$are directly related to the mesh density along the overlap [35]. For a spring element located at an abscissa $x$along the overlap, the stiffnesses are computed from the actual value of adhesive peel and shear modulus, the adhesive thicknesses t_i, the width $b$and the mesh density $\frac{L}{n_{BE}}$such as:

$$\begin{cases} k_{v,i} = m(x)\dfrac{L}{n_{BE}} bk_{I,i} \\ k_{u,i} = m(x)\dfrac{L}{n_{BE}} bk_{II,i} \end{cases} \tag{28}$$

where $m(0 < x < L) = 1$and $m(x = 0) = m(x = L) = \frac{1}{2}$.

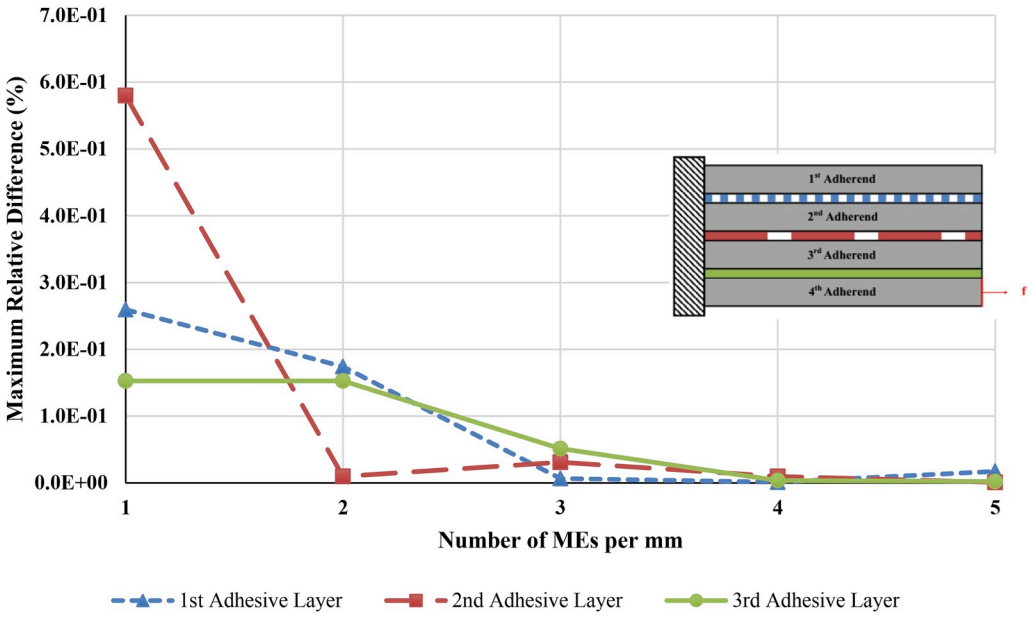


Fig. 11. Maximum relative difference between FE and ME adhesive peak peel stress predictions by 1D-beam model in terms of the number of MEs used per mm.

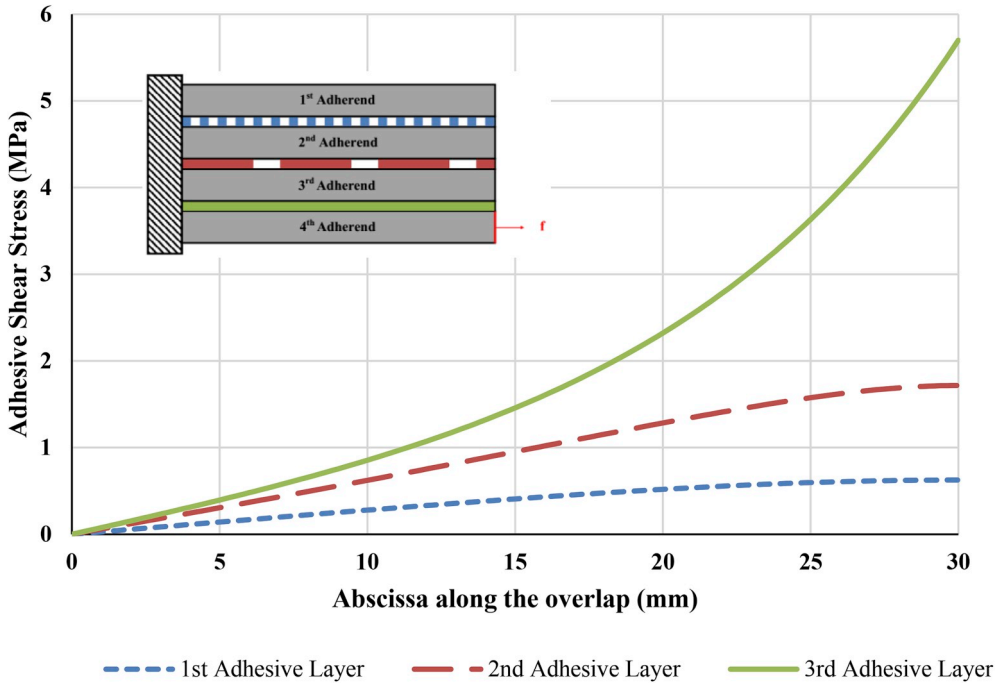


Fig. 12. Adhesive shear stress distribution from 1D-bar ME model along the overlap.

The FE models were developed in SAMCEF v171 FE code. All the details and convergence studies of the FE model are available Ref. [29]. In the present paper, a number of bar or beam elements is then chosen equal to 600 for $L = 30$ *mm*leading to a mesh density of 20 elements per mm providing convergent results.

3.3. *Validation of 1D-bar ME*

Before mesh influence study, the relevance of 1D-bar model is assessed in terms of the symmetry of the stiffness matrix and model restriction by a single-lap joint which has the elementary stiffness matrix determined analytically [19,22]. Firstly, the symmetry of the elementary stiffness matrix is checked by computing the relative difference between each element of the matrix and the corresponding elements of its transpose. A maximal relative difference of 1.93×10^{-13}% is computed using the geometrical and mechanical properties provided in Tables 1–3. Secondly, the model is restricted with the single-lap joint. The relative difference is computed 6.13×10^{-13}% from the maximum difference between the elements of the stiffness matrices of the ME model and analytical model provided in Refs. [19,22]. These small relative differences indicate that the model is well-implemented. Following this, the mesh influence study is studied with FE predictions in order to justify the ME model. Mesh refinement is carried out by a density of mesh per mm. 5 different tests are performed using 1, 2, 3, 4 and 5 MEs per mm. The maximal adhesive shear stresses $T_{max}$and relative differences between T_{max}predicted by 1D-bar ME model and those

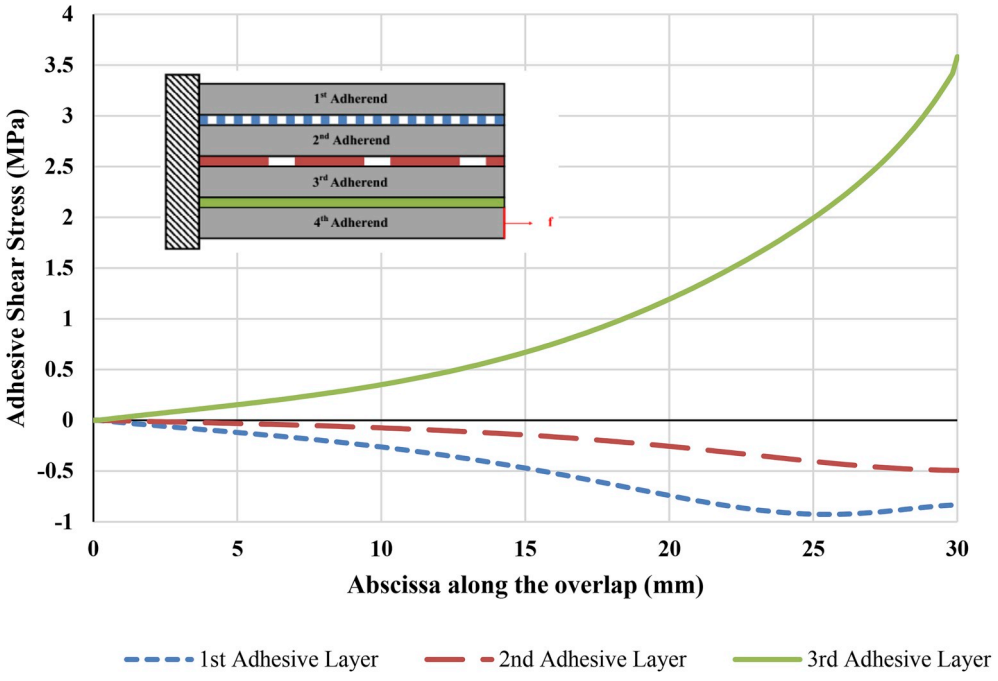


Fig. 13. Adhesive shear stress distribution from 1D-beam ME model along the overlap.

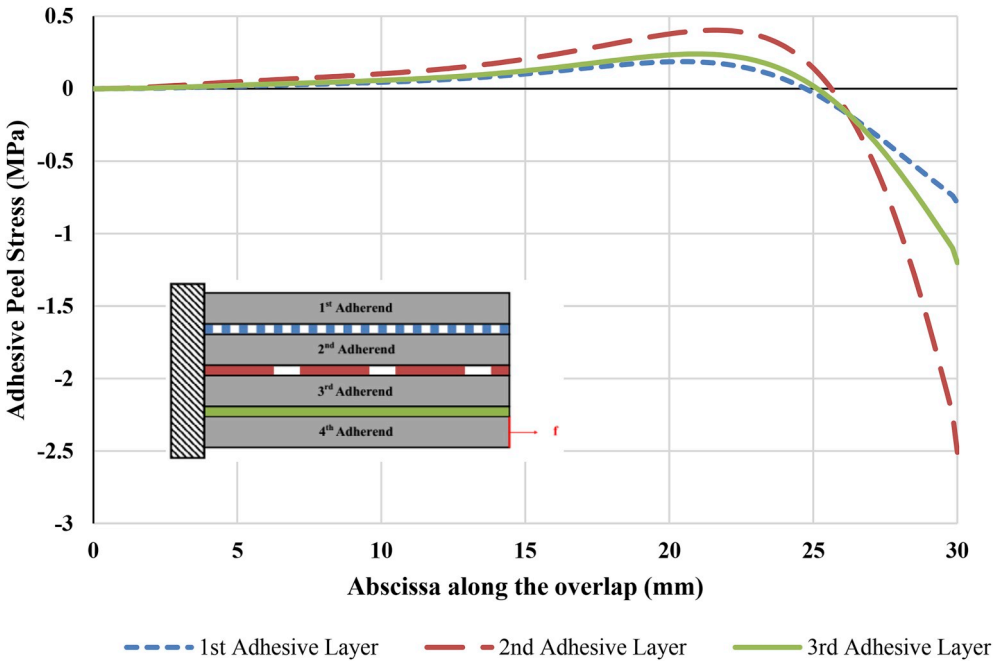


Fig. 14. Adhesive peel stress distribution from 1D-beam ME model along the overlap.

predicted by 1D-bar FE model are provided in Table A-1 and Table A-2 (Appendix A), respectively. It can be seen in Fig. 9 that as the number of MEs per mm increases, these relative differences almost remain constant. A maximal relative difference of 0.02% is computed and it is observed in the 3rd adhesive layer. Figure B-1 (Appendix B) shows that the adhesive stress distributions of 1D-bar FE and 1D-bar ME models appear as superimposed along the overlap using 1 MEs per mm. Good agreement is shown because the FE model assumes the same hypotheses as the ME model. The linear elastic semi-analytical analyses are independent of the mesh refinement in the frame of 1D-bar kinematics.

3.4. Validation of 1D-beam ME

In the frame of 1D-beam kinematics, mesh influence study is studied with FE predictions in order to justify the ME model. Similar to 1D-bar ME model, mesh refinement is carried out by a density of mesh per mm. 5 different tests are performed using 1, 2, 3, 4 and 5 MEs per mm. The maximal adhesive shear stresses T_{max} and peel stresses S_{max} and relative differences between T_{max} and S_{max} predicted by 1D-beam ME model and those predicted by 1D-beam FE model are provided in Tables A-3, A-4, A-5 and A-6 (Appendix A). As the number of MEs per mm increases, these relative differences firstly decrease and then almost remain

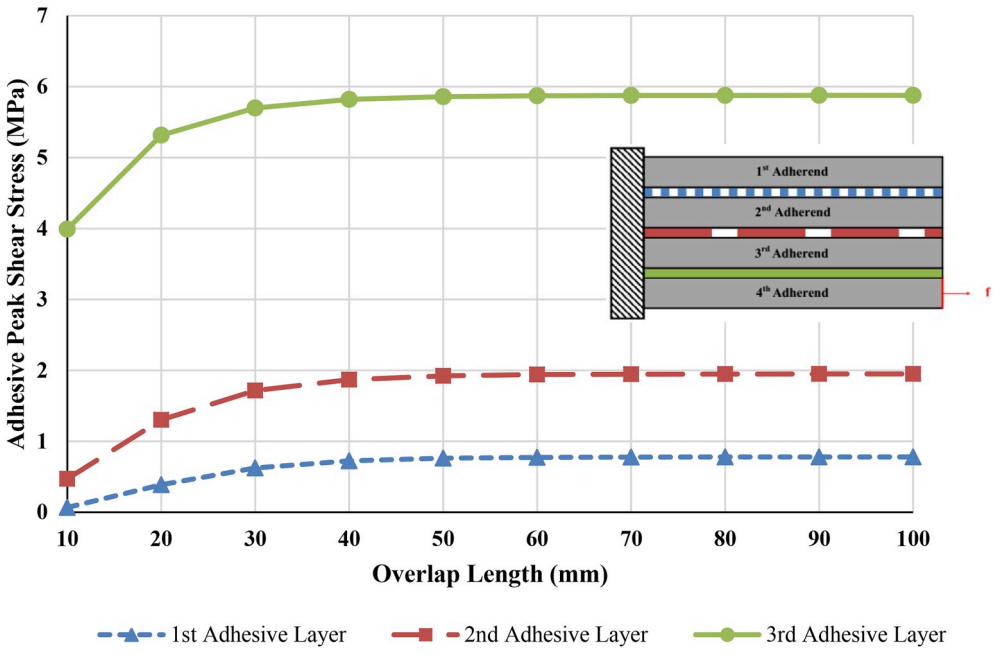


Fig. 15. Adhesive peak shear stress as a function of the overlap length in the case of 1D-bar ME model.

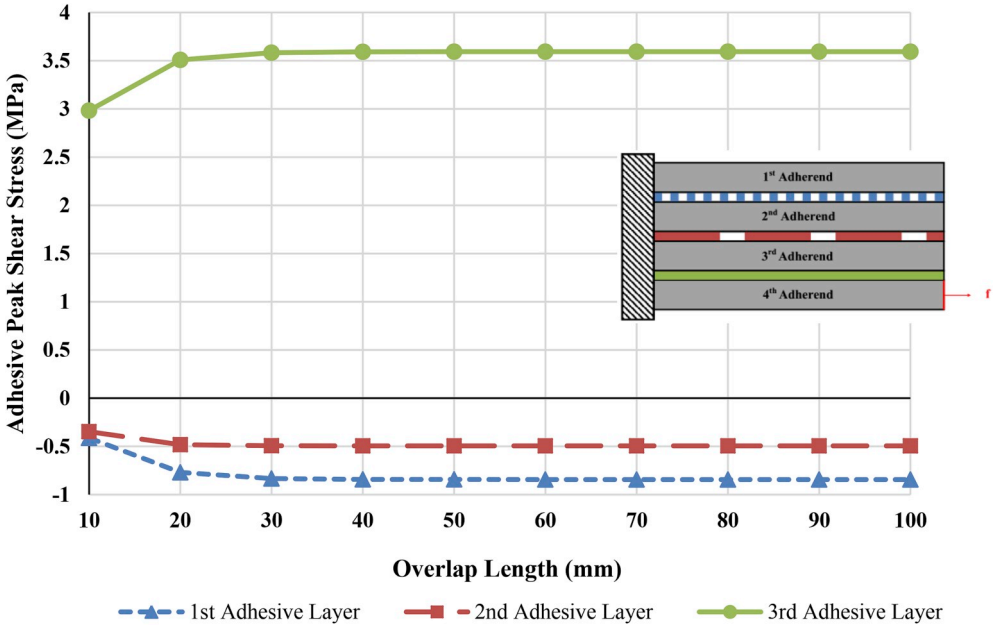


Fig. 16. Adhesive peak shear stress as a function of the overlap length in the case of 1D-beam ME model.

constant, as shown in Figs. 10 and 11. A maximal relative difference of 57.98% is computed for comparison between 1D-beam ME and FE in terms of S_{max} and it is observed in the 1st adhesive layer with the stress analysis of 1 ME per mm. By increasing the mesh density, this relative difference is quickly reduced to 0.09%. Figures B-2 and B-3 (Appendix B) exhibit that the adhesive stress distributions of 1D-beam FE and 1D-beam ME models appear as superimposed along the overlap using a high number of MEs per mm. The analysis results depend on the mesh refinement in the frame of 1D-beam kinematics due to the exponential matrix. Also, 1D-beam kinematics hypotheses lead to a different shape in adhesive shear stresses compared to 1D-bar kinematics.

4. Mechanical behavior

4.1. Mechanical behavior (nominal test case)

The geometrical and mechanical parameters under consideration are given in Tables 1–3. In order to understand the mechanical behavior of the adhesive layers under nominal test case conditions, the adhesive shear and peel stresses obtained with the presented 1D-bar and 1D-beam model are shown in Figs. 12–14. For the nominal test case in the frame of 1D-bar kinematics, the adhesive shear stresses along the overlap rise to a high point and peaked at the end of the overlap. The stress values of the last adhesive layer are much higher than the first and middle adhesive layers because of the chosen adherend layer for the applied force.

The presented 1D-beam model shows different adhesive shear

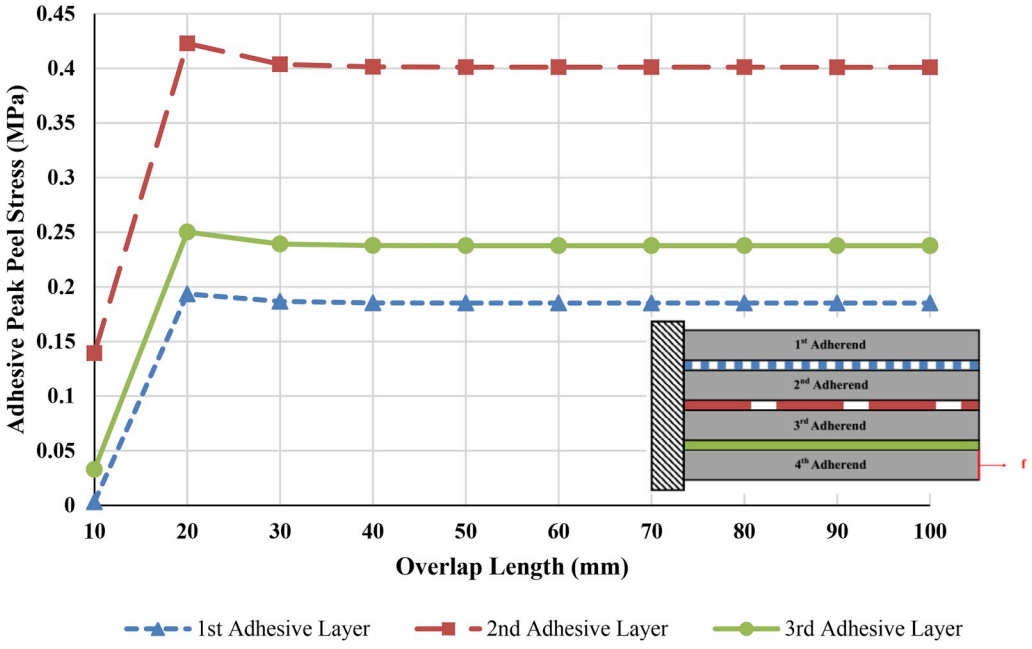


Fig. 17. Adhesive peak peel stress as a function of the overlap length in the case of 1D-beam ME model.

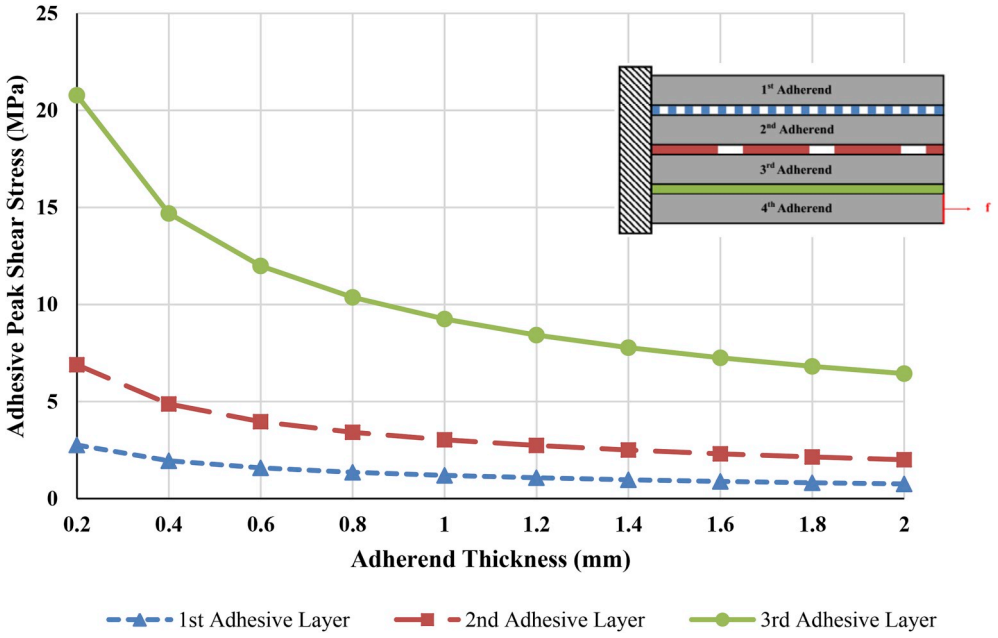


Fig. 18. Adhesive peak shear stress as a function of the adherend thickness in the case of 1D-bar ME model.

distribution compared to 1D-bar model due to the kinematic hypotheses taken. Fig. 13 reveals that the last adhesive layer has similar mechanical behavior whereas the adhesive shear stress distribution along the overlap of the first and the middle adhesive layer is located in the negative area. In addition, what can be clearly seen in Fig. 14 is the maximum adhesive peak peel stress in the middle adhesive layer.

4.2. *Influence of overlap length*

As an application of the simplified stress analyzed based on ME models, the influence of the overlap length on the maximal adhesive shear stress of multilayered adhesively bonded joint is studied considering fixed mesh density as 10 MEs per mm. The analyses are conducted for the overlap lengths from 10 mm to 100 mm by an increase of 10 mm. Within 1D-bar framework, as the overlap lengths of 3 interfaces increase, the maximal adhesive shear stresses increase, and then tend to be a finite value as shown in Fig. 15. Therefore, it is not useful to increase the overlap length to decrease maximal shear stress. As Fig. 16 shows, as the overlap length in the presented 1D-beam model increases, the maximal adhesive shear stress of the third adhesive layer increases above x-axis while the maximal adhesive shear stresses of the first and second adhesive layers slightly increase below x-axis. These peak shear stresses remain stable above a certain value of the overlap length. As for the adhesive peak peel stresses for three adhesive layers shown in Fig. 17, the maximum stresses reach a peak at $L = 20\,mm$. After the peak, what stands out is that the maximum peel stresses decrease and

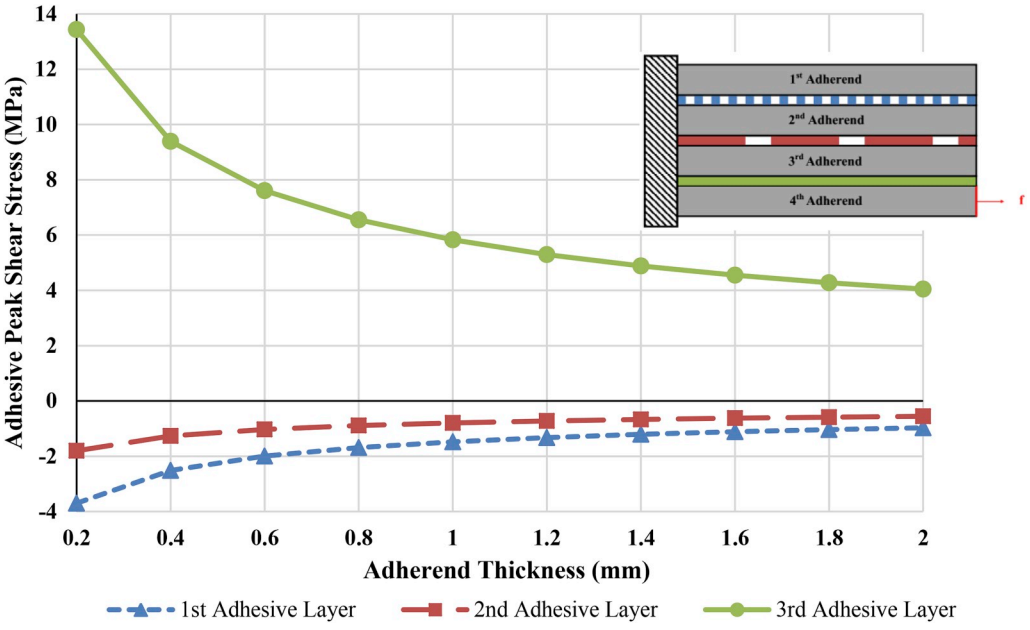


Fig. 19. Adhesive peak shear stress as a function of the adherend thickness in the case of 1D-beam ME model.

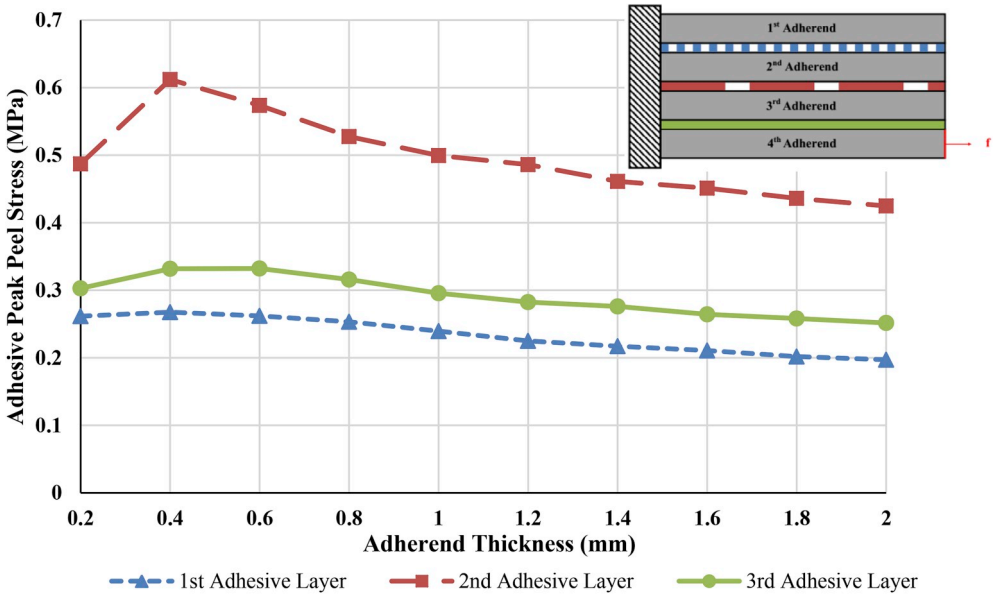


Fig. 20. Adhesive peak peel stress as a function of the adherend thickness in the case of 1D-beam ME model.

then tend to be a finite value above 30 mm. It can be concluded that it is not profitable to increase the overlap length to decrease adhesive maximal peel stress. Also, the mechanical behavior along the overlap has the same adhesive stress distributions in both 1D-bar and 1D-beam models in terms of different overlap lengths as presented in Figs. 12–14.

4.3. Influence of adherend thickness

The adhesive peak stresses as a function of the adherend thickness are given in Figs. 18–20. In order to understand the effect of the adherend thickness on the adhesive peak stresses, the mechanical analyses are performed for different adherend thicknesses from 0.2 mm to 2 mm by an increase of 0.2 mm. For 1D-bar model shown in Fig. 18, as the thickness of the adherends increases, the peak shear stresses of all interfaces decrease and then tend to be a finite value. Therefore, it is not useful to use thicker adherends above a certain value to decrease the maximal shear stress in the case of multilayered bonded joints. Within 1D-beam scheme, the use of thicker adherends leads to a reduction in the maximal adhesive shear stress of the three adhesive layers but then these peak stresses remain stable, as shown in Fig. 19. Fig. 20 shows that there has been a sharp increase up to 0.4 mm of adherend thickness on the maximum adhesive peel stress of second adhesive layer by increasing the adherend thickness. After reaching a peak around 0.4 mm, these maximum peel stress continuously decrease. Compared to the second adhesive layer, there has been a slight decrease in the first and third adhesive layer. After the peak value at 0.4 mm of the adherend thickness, maximum adhesive peel stresses fall in the three adhesive layers while the drop in the second adhesive layer is sharper than others. This non-monotonic behavior remains unexplained. It can be deduced that the maximum peel stress can be reduced by increasing the adherend thickness. In addition, for different adherend thicknesses, the stress distributions along the overlap vary as presented in Figs. 12–14.

5. Conclusion

This paper set out to perform the stress analysis of the multilayered adhesively bonded joints using a semi-analytical resolution method. The second aim of this study was to investigate the effects of the different parameters in order to understand the mechanical behavior of multilayered adhesively bonded joints. A comparison between simplified and refined stress analyses of multilayered adhesively bonded structures subjected to pure mechanical tensile in-plane loading is presented. The simplified stress analyses are performed using 1D-bar and 1D-beam kinematics in order to predict the mechanical behavior of such joints. The ME technique is a semi-analytical resolution method used for the simplified stress analysis. Firstly, the simplified approach based on simplifying hypotheses is developed to model the joints. The ME technique is the resolution scheme used for the simplified stress analysis. A multilayered bonded-bars and a multilayered bonded-beams MEs are derived in the frame of linear elastic adhesive behavior. The detailed mathematical derivation is presented. For the purpose of validation, the results obtained by the simplified 1D-bar and 1D-beam MEs are compared with the results predicted by 1D-FE models [29]. Mesh influence studies are performed using different mesh densities in order to validate the ME mode. Relative differences between 1D-FE and 1D-ME models for different mesh densities are computed in terms of adhesive stresses. The results of this study show that the method is validated by 1D-FE model by computing small relative differences. These results, therefore, need to be interpreted with the caution that 1D-FE and 1D-ME models assume the same hypotheses and these hypotheses lead to the same results for 1D-bar model and close results for 1D-beam model. For 1D-beam model, it is found that there is a dependency on the number of MEs. Finally, parametric studies of 1D-ME models are presented consisting of the analysis of the influence of the overlap length and the adherend thickness. The outputs of these parametric studies are taken as adhesive peak shear and peel stresses in order to evaluate the results. The findings of this research provide insights for the computational time in the use of ME technique. This semi-analytical resolution has the advantage of the computational time for the small mesh sizes and so high number of elements through software code developed for the numerical analysis. Furthermore, the number of layers is not a restriction because a different number of layers are able to be simulated depending on the requirements. This presented simplified stress analysis will be of interest to deduce the sizing guidelines in order to perform the preliminary design. More broadly, further research in this field would be needed to determine the mechanical analysis of non-linear adhesive behavior.

Acknowledgment

This work has not received any specific grant.

Appendix A. Supplementary data

Supplementary data to this article can be found online at https://doi.org/10.1016/j.ijadhadh.2019.102497.

References

[1] Hart-Smith LJ. Design methodology for bonded-bolted composite joints. Volume I. Analysis derivations and illustrative solutions. California: Long Beach; 1982.
[2] Higgins A. Adhesive bonding of aircraft structures. Int J Adhesion Adhes 2000;20:367–76. https://doi.org/10.1016/S0143-7496(00)00006-3.
[3] Kelly G. Quasi-static strength and fatigue life of hybrid (bonded/bolted) composite single-lap joints. Compos Struct 2006;72:119–29. https://doi.org/10.1016/j.compstruct.2004.11.002.
[4] da Silva LFM, Öchsner A, Adams RD. Handbook of adhesion technology. second ed., vols. 1–2. Heidelberg: Springer; 2018. https://doi.org/10.1007/978-3-319-55411-2.
[5] van Ingen JW, Vlot A. Stress analysis of adhesively bonded single lap joints. (Report LR-740). Delft Univ Technol; 1993.
[6] Tsai MY, Morton J. An evaluation of analytical and numerical solutions to the single-lap joint. Int J Solids Struct 1994;31:2537–63. https://doi.org/10.1016/0020-7683(94)90036-1.
[7] da Silva LFM, das Neves PJC, Adams RD, Spelt JK. Analytical models of adhesively bonded joints - Part I: literature survey. Int J Adhesion Adhes 2009;29:319–30. https://doi.org/10.1016/j.ijadhadh.2008.06.005.
[8] Volkersen O. Die Nietkraftverteilung in zugbeanspruchten Nietverbindungen mit konstanten Laschenquerschnitten. Luftfahrtfor Schung 1938;15:41–7.
[9] Goland M. The stresses in cemented joints. J Appl Mech 1944;17.
[10] Hart-Smith LJ. Adhesive-bonded scarf and stepped-lap joints. California: Long Beach; 1973.
[11] Hart-Smith LJ. Adhesive-bonded single-lap joints. California: Long Beach; 1973.
[12] Hart-Smith LJ. Adhesive-bonded double-lap joints. California: Long Beach; 1973.
[13] Bigwood DA, Crocombe AD. Elastic analysis and engineering design formulae for bonded joints. Int J Adhesion Adhes 1989;9:229–42. https://doi.org/10.1016/0143-7496(89)90066-3.
[14] Oplinger DW. A layered beam theory for single lap joints. 1991.
[15] Tsai MY, Oplinger DW, Morton J. Improved theoretical solutions for adhesive lap joints. Int J Solids Struct 1998;35:1163–85. https://doi.org/10.1016/S0020-7683(97)00097-8.
[16] Alfredsson KS, Högberg JL. A closed-form solution to statically indeterminate adhesive joint problems-exemplified on ELS-specimens. Int J Adhesion Adhes 2008;28:350–61. https://doi.org/10.1016/j.ijadhadh.2007.10.002.
[17] Luo Q, Tong L. Fully-coupled nonlinear analysis of single lap adhesive joints. Int J Solids Struct 2007;44:2349–70. https://doi.org/10.1016/j.ijsolstr.2006.07.009.
[18] Weißgraeber P, Stein N, Becker W. A general sandwich-type model for adhesive joints with composite adherends. Int J Adhesion Adhes 2014;55:56–63. https://doi.org/10.1016/j.ijadhadh.2014.06.009.
[19] Paroissien E. Contribution aux assemblages hybrides (Boulonnés/Collés) – application aux jonctions aéronautiquesvol. III. Université de Toulouse; 2006.
[20] Paroissien E, Sartor M, Huet J. Hybrid (bolted/bonded) joints applied to aeronautic parts: analytical one-dimensional models of a single-lap joint. In: Tichkiewitch S, Tollenaere M, Ray P, editors. Adv. Integr. Des. Manuf. Mech. Eng. II. Dordrecht: Springer; 2007. p. 95–110.
[21] Paroissien E, Sartor M, Huet J, Lachaud F. Analytical two-dimensional model of a hybrid (Bolted/Bonded) single-lap joint. J Aircr 2007;44:573–82. https://doi.org/10.2514/1.24452.
[22] Paroissien E, Lachaud F, Jacobs T. A simplified stress analysis of bonded joints using macro-elements. In: Kumar S, Mittal KL, editors. Advances in modeling and design of adhesively bonded bonded systems. Adv. Model. Des. Adhes. Bond. Syst., Beverly: Wiley-Scrivener; 2013. p. 93–146. https://doi.org/10.1002/9781118753682.
[23] Paroissien E, Gaubert F, Da Veiga A, Lachaud F. Elasto-plastic analysis of bonded joints with macro-elements. J Adhes Sci Technol 2013;27:1464–98. https://doi.org/10.1080/01694243.2012.745053.
[24] Lelias G, Paroissien E, Lachaud F, Morlier J, Schwartz S, Gavoille C. An extended semi-analytical formulation for fast and reliable mode I/II stress analysis of adhesively bonded joints. Int J Solids Struct 2015;62:18–38. https://doi.org/10.1016/j.ijsolstr.2014.12.027.
[25] Paroissien E, Lachaud F, Schwartz S, Da Veiga A, Barrière P. Simplified stress analysis of hybrid (bolted/bonded) joints. Int J Adhesion Adhes 2017;77:183–97. https://doi.org/10.1016/j.ijadhadh.2017.05.003.
[26] Paroissien E, Lachaud F, Morlier J, Schwartz S. A direct method for the assessment of cohesive zone models for thin adhesive layers loaded in mode I, mode II, and mixed-mode I/II. Rev Adhes Adhes 2018. https://doi.org/10.7569/raa.2018.097301.
[27] Paroissien E, da Silva LFM, Lachaud F. Simplified stress analysis of functionally graded single-lap joints subjected to combined thermal and mechanical loads. Compos Struct 2018;203:85–100. https://doi.org/10.1016/j.compstruct.2018.07.015.
[28] Lélias G, Paroissien E, Lachaud F, Morlier J. Experimental characterization of cohesive zone models for thin adhesive layers loaded in mode I, mode II, and mixed-mode I/II by the use of a direct method. Int J Solids Struct 2019;158:90–115. https://doi.org/10.1016/j.ijsolstr.2018.09.005.
[29] Paroissien E, Lachaud F, da Silva LFM, Seddiki S. A comparison between macro-element and finite element solutions for the stress analysis of functionally graded single-lap joints. Compos Struct 2019;215:331–50. https://doi.org/10.1016/j.compstruct.2019.02.070.
[30] Nairn JA, Mendels DA. On the use of planar shear-lag methods for stress-transfer analysis of multilayered composites. Mech Mater 2001;33:335–62. https://doi.org/10.1016/S0167-6636(01)00056-4.
[31] Jiang G, Peters K. A shear-lag model for three-dimensional, unidirectional multilayered structures. Int J Solids Struct 2008;45:4049–67. https://doi.org/10.1016/j.ijsolstr.2008.02.018.
[32] Viet NV, Zaki W, Umer R. Interlaminar shear stress function for adhesively bonded multi-layer metal laminates. Int J Adhesion Adhes 2018;82:14–20. https://doi.org/10.1016/j.ijadhadh.2017.12.011.
[33] Pham P Van, Mohareb M, Fam A. Finite element formulation for the analysis of multilayered beams based on the principle of stationary complementary strain energy. Eng Struct 2018;167:287–307. https://doi.org/10.1016/j.engstruct.2018.04.014.
[34] Simo JC, Laursen TA. An augmented Lagrangian treatment of contact problems involving friction. Comput Struct 1992;42:97–116. https://doi.org/10.1016/0045-7949(92)90540-G.
[35] Dechwayukul C, Rubin CA, Hahn GT. Analysis of the effects of thin sealant layers in aircraft structural joints. AIAA J 2003;41:2216–28.